Supplementary information of Spectroscopic signatures of nonpolarons: the case of diamond

Joao C. de Abreu[1], Jean Paul Nery[2], Matteo Giantomassi[3], Xavier Gonze[3,4], and Matthieu J. Verstraete[1]

[1]nanomat/Q-MAT/CESAM and European Theoretical Spectroscopy Facility, Université de Liège, B-4000 Belgium
[2]Dipartimento di Fisica, Università di Roma La Sapienza, I-00185 Roma, Italy
[3]UCLouvain, Institute of Condensed Matter and Nanosciences (IMCN), Chemin des Étoiles 8, B-1348 Louvain-la-Neuve, Belgium
[4]Skolkovo Institute of Science and Technology, Moscow, Russia

S.1 Electronic and phonon structure

The non-interacting wave-functions $\psi^0_{n\mathbf{k}}$ and eigenvalues $\varepsilon^0_{n\mathbf{k}}$ are determined self-consistently from the Kohn-Sham (KS)[1] equation in density functional theory (DFT)[2],

$$[T + v_{\text{ext}}(\mathbf{r}) + v_H[\rho(\mathbf{r})] + v_{\text{XC}}[\rho(\mathbf{r})]]\,\psi^0_{n\mathbf{k}}(\mathbf{r}) = \varepsilon^0_{n\mathbf{k}}\psi^0_{n\mathbf{k}}(\mathbf{r}) \tag{S.1.1}$$

where $\rho(\mathbf{r}) = \sum_{n\mathbf{k}} f_{n\mathbf{k}}|\psi^0_{n\mathbf{k}}(\mathbf{r})|^2$ is the electronic density. Inside the brackets the first term is the kinetic energy operator and the other terms constitutes the KS potential, v^{KS}, composed of (from left to right): the external potential, the Hartree energy potential, and the exchange-correlation potential.

DFPT is used to calculate the interatomic forces constants, which are the second derivative of the total energy with respect to atomic displacements. The phonon frequencies $\omega_{j\mathbf{q}}$ and the eigendisplacements $U_{j\mathbf{q}}$ are thus obtained as solutions of the generalized eigenvalue problem[3] involving the dynamical matrix $C(\mathbf{q})$,

$$\sum_{\kappa'\beta} C_{\kappa\alpha,\kappa'\beta}(\mathbf{q})U_{j\mathbf{q}}(\kappa'\beta) = M_\kappa\omega^2_{j\mathbf{q}}U_{j\mathbf{q}}(\kappa\alpha) \tag{S.1.2}$$

where M is the atomic mass, κ and κ' are the index of the ions in the unit cell, j is the phonon mode, and α and β are the Cartesian directions. The e-ph matrix elements are derived from the first order variation of the KS potential, and given by

$$g^{j\mathbf{q}}_{nm\mathbf{k}} = \int d\mathbf{r}\left(\psi^0_{n\mathbf{k}+\mathbf{q}}(\mathbf{r})\right)^* \frac{e^{i\mathbf{q}\cdot\mathbf{r}}}{\sqrt{2\omega_{j\mathbf{q}}}} \times \sum_{\kappa\alpha}\frac{U_{\kappa\alpha,j}(\mathbf{q})}{\sqrt{M_\kappa}}\left(\partial_{\kappa\alpha,\mathbf{q}}v^{KS}(\mathbf{r})\right)\psi^0_{m\mathbf{k}}(\mathbf{r}). \tag{S.1.3}$$

The first-order derivative of v^{KS} is obtained by solving self-consistently a system of Sternheimer equations. All these calculations give us the quantities necessary to compute the e-ph self-energy.

S.2 Computational details

We performed calculations for the KS band structure using the LDA approximation[4,5]. Core electrons were taken into account using a norm-conserving pseudopotential[6]. The electronic wave functions were expanded in plane-wave basis set with an energy cutoff of 40 Ha. Phonon properties together with the e-ph scattering potentials were calculated by means of DFPT and a $8 \times 8 \times 8$ grid both for electrons and phonons. Then we performed MBPT calculations to determine the e-ph correction to the initial LDA electronic structure. ABINIT[7,8] was used for all the calculations.

Diamond atoms have tetrahedral geometry and bond via sp^3 hybrid orbitals. There are two atoms per unit cell, with a relative displacement of $(1/4, 1/4, 1/4)a$, where a is the lattice parameter. The unit cell of diamond is shown in Fig. S.2.1. The relaxed structure has $a = 3.575$ Å, differing by 0.16% from the experimental value[9]. The calculated fundamental band gap of diamond is 4.173 eV and the direct band gap is 5.610 eV. Calculations at the LDA level are known to underestimate the band gap, in this case, the errors are around 24% and 21%, respectively[10].

The phonon band structure is shown in Fig. S.2.2. Although there is no LO-TO splitting since diamond is not polar, we refer to the largest phonon frequency at Γ as ω_{LO} (163 meV).

The convergence of the phonon energy with respect to the initial DFPT q-grid show a maximum of 0.04 meV for a size of $8 \times 8 \times 8$. A denser $\mathbf{q}$-mesh does not affect much the spectral function for CBM at the examined temperatures of 300, 900 and 1500 K. However, further convergence might be needed for transport properties[11].

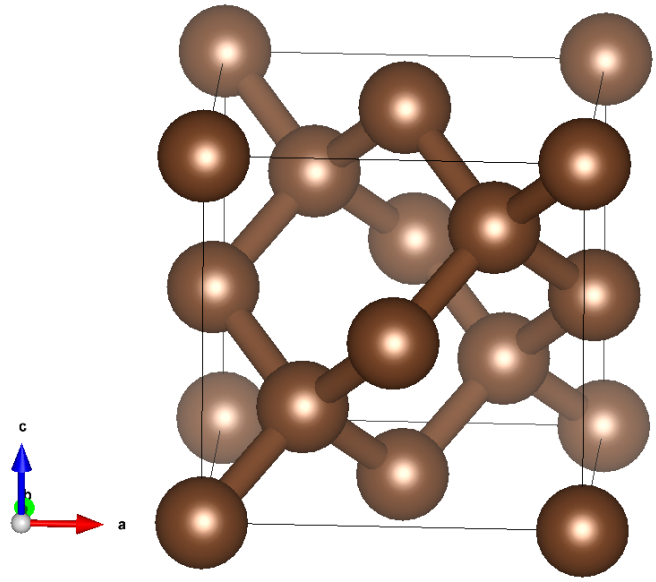

Figure S.2.1 The conventional 8 atom cubic unit cell of diamond. The calculations were done using 2 atoms in a face-centred cubic primitive unit cell.

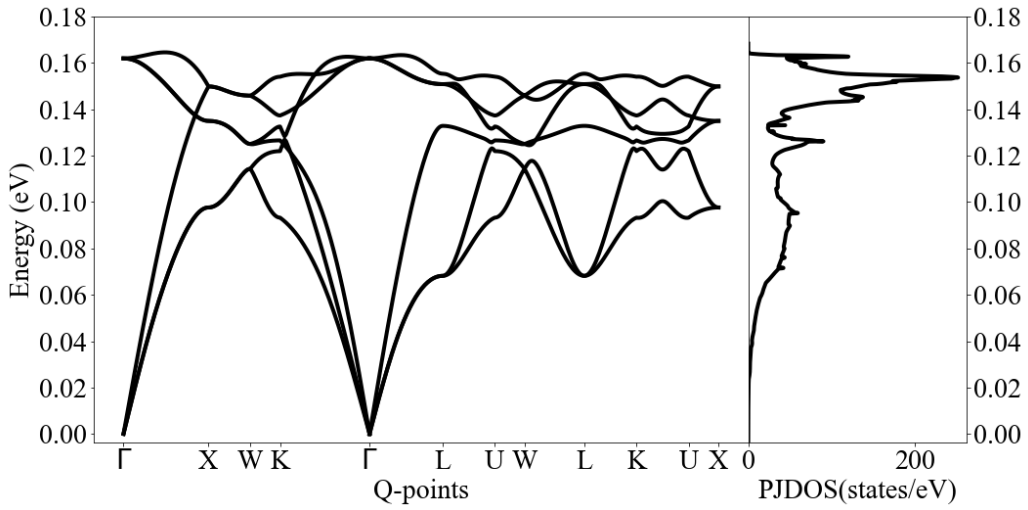

Figure S.2.2 The phonon band structure (left) and density of states (right) of diamond obtained by Fourier-interpolating the dynamical matrix evaluated on a $8 \times 8 \times 8$ $\mathbf{q}$-grid.

S.3 Kramers-Kronig

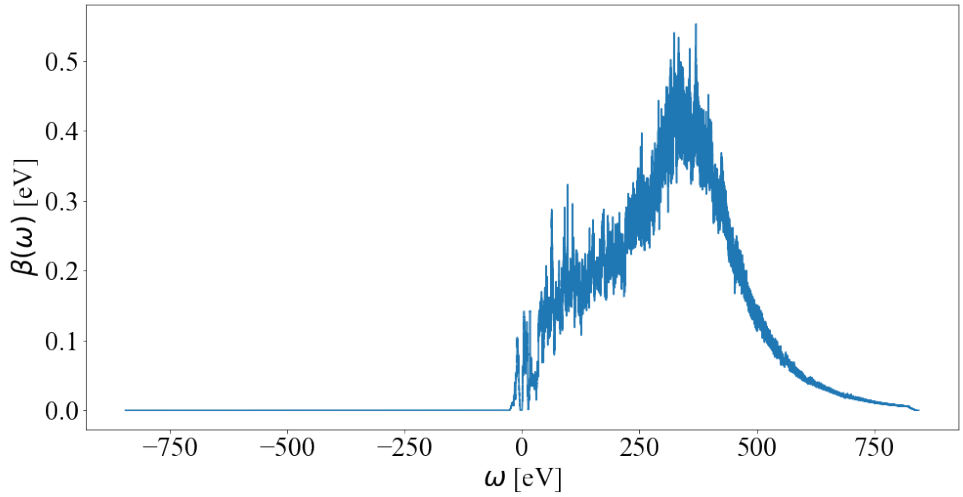

Figure S.3.1 $\beta_{\mathrm{CBM}}(\omega)$ using a $64 \times 64 \times 64$ $\mathbf{k}$- and $\mathbf{q}$-grid with a total of 650 bands. For this calculation, the infinitesimal number η is of 10 meV.

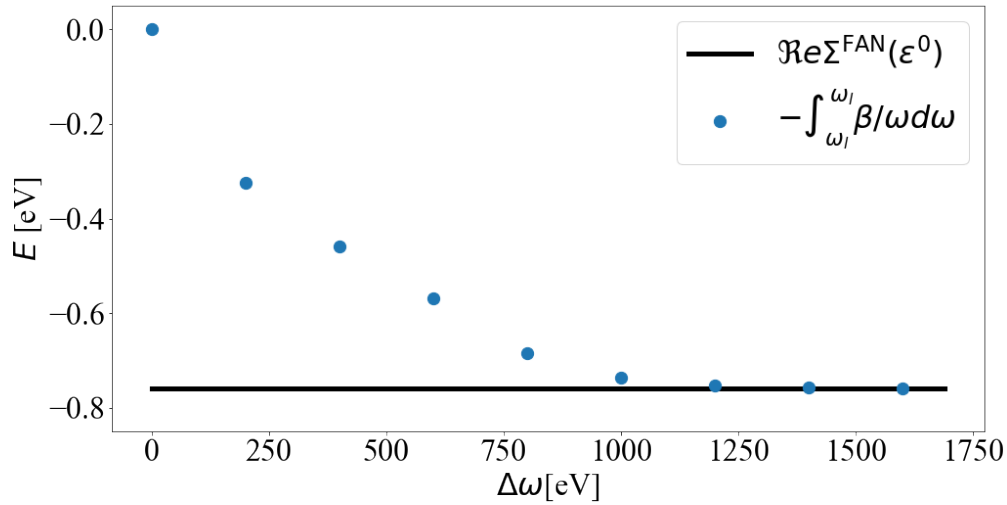

Figure S.3.2 The integration of $\beta_{\mathrm{CBM}}(\omega)/\omega$ ($\beta_{\mathrm{CBM}}(\omega)$ from Fig. S.3.1) between $-\omega_l$ and ω_l ($\Delta\omega$) converges at a large value of $\Delta\omega$, of about 700 eV. The converged value corresponds to the real part of the Fan self-energy at $\omega = \varepsilon^0_{\mathrm{CBM}}$ due to the Kramers-Kronig (KK) relation, Eq. (S.3.1). To reduce the computational cost, one can just use KK and avoid the numerical integration of the $\beta_{\mathrm{CBM}}(\omega)/\omega$ term in Eq. (9).

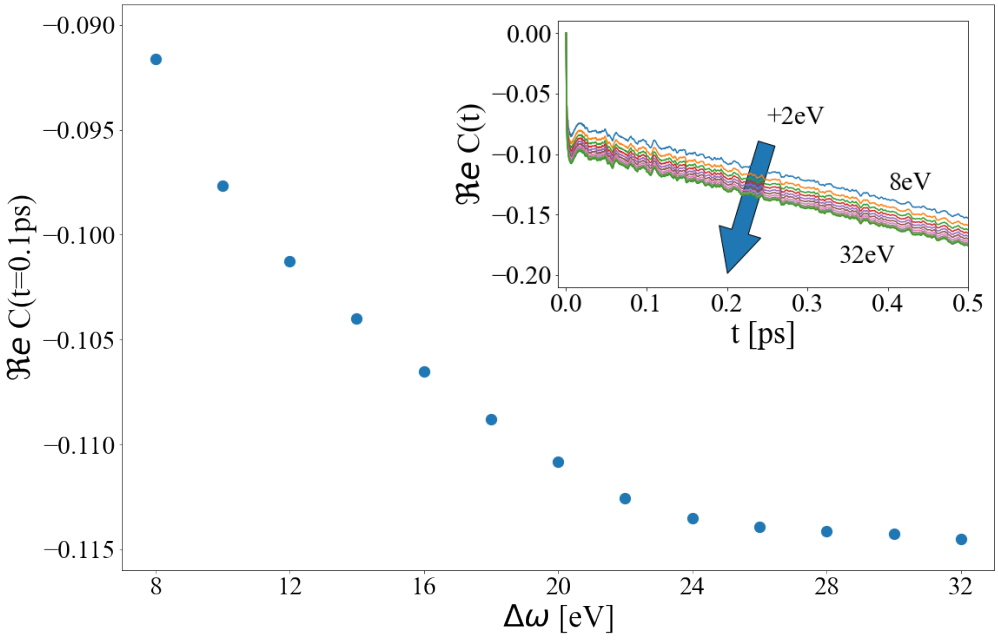

Figure S.3.3 Convergence of $\Re e\tilde{C}(t = 0.1\mathrm{ps})$ at the CBM, from Eq. (S.3.2), with respect to the frequency integration range $\Delta\omega$. There is a convergence of 0.001 at $\Delta\omega = 22$ eV, which corresponds to 8 bands, and the imaginary part is converged already at $\Delta\omega = 8$ eV. The inset shows $\Re e\tilde{C}(t)$ for different integration ranges. The lines with a decreasing y-intercept are calculated for frequency ranges $\Delta\omega$ increasing by 2 eV, from 8 eV and 32 eV, which yields a converging rigid shift of $\Re e\tilde{C}(t)$.

Converging the ω-integral in Eq. (9) requires a very large integration range. In Fig. S.3.1 we can see that the imaginary part of the self-energy does not have a small support of ω around $\varepsilon_{n\mathbf{k}}$, but continues to increase up to about 400 eV, and does not go to 0 until values well over 700 eV. In addition, one of the the cumulant terms, $\int \beta/\omega d\omega$, has a factor $1/\omega$ rather than $1/\omega^2$, which makes convergence very slow. In fact, Fig. S.3.2 shows that $\Delta\omega$ =800 eV is needed to converge the integral with an accuracy of 0.01 eV, which corresponds to about 630 bands. This can be avoided by using the Kramers-Kronig (KK) relation,

$$\Re e\Sigma^{\text{Fan}}_{n\mathbf{k}}(\varepsilon_{n\mathbf{k}}) = -P\int_{\infty}^{\infty}\frac{\beta_{n\mathbf{k}}(\omega)}{\omega}d\omega. \tag{S.3.1}$$

where P indicates the Cauchy principal value. Using this analytical result, the numerical integration of the $1/\omega$ term is completely avoided. In this way, we can write

$$\begin{aligned} C_{n\mathbf{k}}(t) &= -it\Re e\Sigma^{\text{Fan}}_{n\mathbf{k}}(\varepsilon_{n\mathbf{k}}) + P\int_{-\infty}^{\infty}\beta_{n\mathbf{k}}(\omega)\frac{e^{-i\omega t}-1}{\omega^2}d\omega \\ &= -it\Re e\Sigma^{\text{Fan}}_{n\mathbf{k}}(\varepsilon_{n\mathbf{k}}) + \tilde{C}_{n\mathbf{k}}(t), \end{aligned} \tag{S.3.2}$$

which is the expression used in our calculations. On the other hand, $\tilde{C}(t)$ at $t = 0.1$ ps is converged by integrating up to 15 eV (see Fig. S.3.3), which requires the explicit calculation of only 9 bands. For larger values of t, the range of energy is even smaller.

The issue of converging the cumulant has now been reduced to converging the real part of the self-energy in Eq. (S.3.2), given by Eq. 3. In principle, this also requires calculating many bands to converge the sum m. However, calculating the self-energy is now a standard tool in ABINIT and other first-principles codes, where the sum over bands is usually avoided by using the Sternheimer approximation.

S.4 Sternheimer approximation

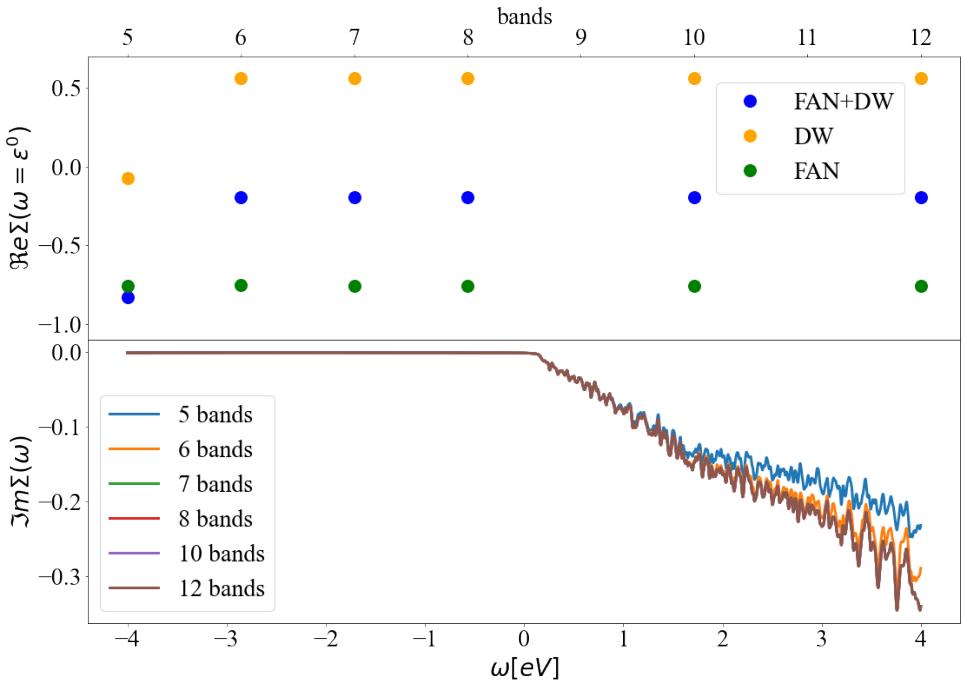

Figure S.4.1 CBM self-energy. Top: Real part at the KS energy as a function of the number of explicit bands M. At $M = 6$ it is already well converged, explicitly showing that the phonon frequencies play only a small role when energy denominators are large. Bottom: Imaginary part of the self energy, as a function of frequency, for different number of bands. Since the imaginary part is not 0 only if $\omega - \varepsilon_{n'\mathbf{k}+\mathbf{q}} \pm \omega_{\mathbf{q}s} = 0$, values agree in the whole range as soon as at least one band is added above 4 eV.

Converging the calculation of the e-ph self-energy requires the inclusion of many empty states. This can be circumvented by using Eqs. (26)-(31) in Ref. 12 , in which the sum for $n' > M$ can be replaced by the numerical solution of the Sternheimer equation. Obtaining the self-energy in this way corresponds, for $m > M$ in Eq. (3), to setting $\omega = \varepsilon_{n\mathbf{k}}$ (which is precisely what is needed in Eq. (S.3.1)) and dropping the phonon frequencies $\omega_{\mathbf{q}s}$ in the denominators. Energy differences $\varepsilon_{n\mathbf{k}} - \varepsilon_{n'\mathbf{k}+\mathbf{q}}$ are much larger than $\omega_{\mathbf{q}s}$, even for m not much larger than n, so dropping the phonon frequencies has virtually no effect.

In Fig. S.4.1, we can see that by using the Sternheimer approximation, $\Re e\Sigma^{\mathrm{Fan}}_{n\mathbf{k}}(\omega = \varepsilon_{n\mathbf{k}})$ is converged by summing explicitly over only 6 bands. In the previous section, we obtained that more bands, 9, are needed to converge $\tilde{C}$ in Eq. (S.3.2), so the method is fully converged by determining only 9 bands of the self-energy. For the VBM, a similar amount of bands are needed.

Regarding the frequency dependence (dynamical effects) of the self-energy, the Sternheimer approximation implies that it is not included for $m > M$. However, if the real part of the self-energy is evaluated close to $\varepsilon_{n\mathbf{k}}$, such that $|\omega - \varepsilon_{n\mathbf{k}}| \ll |\omega - \varepsilon_{n'\mathbf{k}+\mathbf{q}}|$, then this is also a good approximation. For the imaginary part, contributions come from $\omega - \varepsilon_{n'\mathbf{k}+\mathbf{q}} \pm \omega_{\mathbf{q}s} = 0$, so as long as ω takes values slightly lesser than those of the $m > M$ bands, the approximation has no effect, and the spectral function can be accurately determined. Therefore, by using KK, the Sternheimer approximation can be safely used by calculating explicitly the bands up to $m \leq M$, for a small value of M.

S.5 Self-Energy details

The inverse of the Dyson-Migdal equation, eq. 4, is given by

$$\Sigma_{n\mathbf{k}}(\omega;T) = \frac{1}{G^{(0)}_{n\mathbf{k}}(\omega)} - \frac{1}{G_{n\mathbf{k}}(\omega;T)}. \tag{S.5.1}$$

There is a distinct decay between G^0 and the CE calculated G at large ω, which can be seen in Fig. S.5.1. The Fourier Transform used for CE method forces G to zero in the frequency numerical limits and this disparity produces a divergence in Σ as G tends to zero, Fig. S.5.2. Nevertheless, close to the KS energy between -2.0 and 2.0 eV, see Fig. S.5.3, where G and G^0 are close to each other and far from 0 by $\pm$ 0.5 (Fig. S.5.1), the DM and CE self-energies are within the same range of energies. The real part of the self-energy between the QP line (diagonal solid black line) and the plateau energy line (diagonal dashed black line) seems to begin or continue, depending on the temperature, a descending behaviour. However, reaching to a distance of ω_{LO} the descent stops and leads to a plateau. This is at variance with polar materials, where at ω_{LO} the real part of the self-energy diverges.

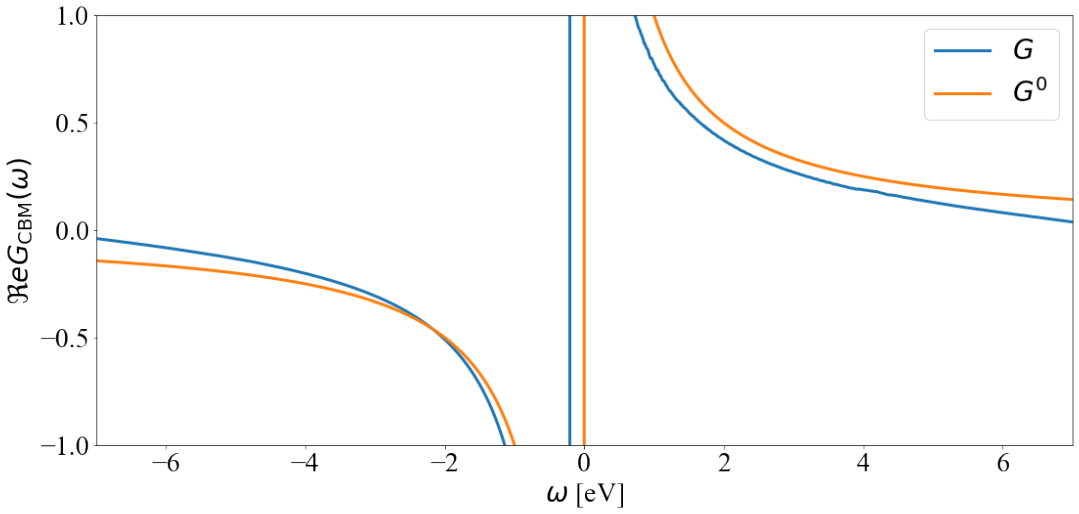

Figure S.5.1 Calculated Green's functions in the frequency domain at CBM. In blue, the total CE Green's function and in orange the non-interacting particle Green's function. The latter has a slower decay to zero (as $1/\omega$) than the former. As the CE G is constructed by Fourier transform, it must be periodic and goes to 0 at the edge of the chosen frequency interval (around $\pm$8 eV).

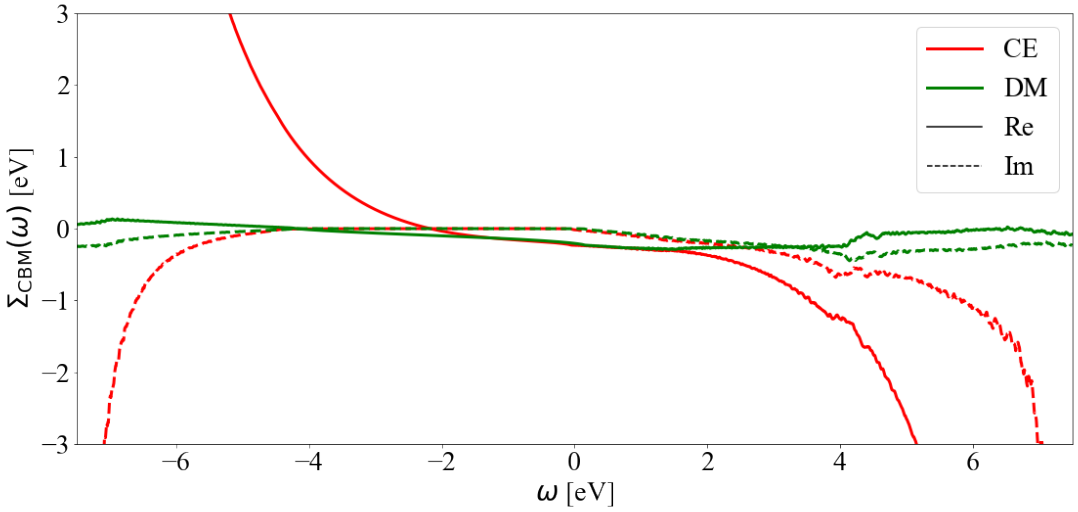

Figure S.5.2 The real (solid) and imaginary (dashed) parts of the self-energy for DM (green) and CE (red) at the CBM. The CE self-energy is calculated as the difference of the inverses of the CE and non-interacting Green's functions, and diverges with increasing ω due to the distinctive decay (faster than $1/\omega$) of the CE Green's function, Fig. S.5.1.

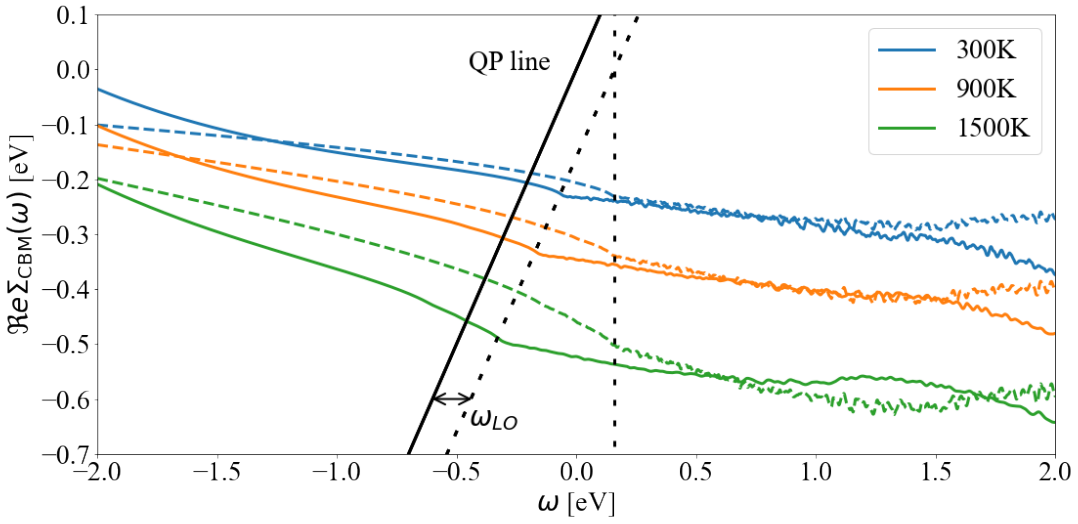

Figure S.5.3 Real part of the self-energy at 300 (blue), 900 (orange), and 1500 (green) K, both for CE (solid) and DM (dashed) calculations at the CBM. The diagonal solid black line shows $\omega = \Re e\Sigma(\omega)$, corresponding to Eq. (13), with $\varepsilon^0_{\mathrm{CBM}}$ set to zero, and intersections with $\Re e\Sigma(\omega)$ yield the QP energy peaks. The diagonal dashed black line is shown at a distance of ω_{LO} from the QP line. The vertical dashed line is set to ω_{LO} from $\varepsilon^0_{\mathrm{CBM}}$. Both dashed black lines highlight the position of the satellite plateau structure, which is physical only in the CE case.

S.6 Spectral function and ARPES

S.6.1 Energy values

Energy values corresponding to Figs. 10 and 11 of the main text are compiled in Table S.6.1.

State	CBM			VBM		
Temperature (K)	300	900	1500	300	900	1500
$\Re e\Sigma^{\mathrm{DW}}_{n\mathbf{k}}(\varepsilon^0_{n\mathbf{k}})$	0.659	1.148	1.779	1.974	3.440	5.333
$\Re e\Sigma^{\mathrm{FAN}}_{n\mathbf{k}}(\varepsilon^0_{n\mathbf{k}})$	-0.862	-1.430	-2.182	-1.841	-3.188	-4.867
$\Re e\Sigma_{n\mathbf{k}}(\varepsilon^0_{n\mathbf{k}})$	-0.203	-0.282	-0.403	0.134	0.252	0.466
$\Im m\Sigma_{n\mathbf{k}}(\varepsilon^0_{n\mathbf{k}})$	-1.5×10^{-4}	-3.5×10^{-3}	-9.4×10^{-3}	-1.1×10^{-3}	-3.9×10^{-2}	-1.1×10^{-1}
ε^{DM-OMS}	-0.203	-0.282	-0.403	0.134	0.252	0.466
$\varepsilon^{DM-Linear}$	-0.187	-0.241	-0.311	0.120	0.171	0.288
ε^{DM-NL}	-0.179	-0.260	-0.367	0.121	0.161	0.221
ε^{CE-NL}	-0.203	-0.282	-0.402	0.134	0.252	0.464

Table S.6.1 Self-energy and energy renormalization values (in eV) at the CBM and VBM for several temperatures. Calculation were done using a $128\times128\times128$ $\mathbf{q}$-grid and $\eta = 5$ meV.

S.6.2 Σ^+ and Σ^-

In Fig. S.6.1, we separate the contributions Σ^+ and Σ^- of the spectral function at the VBM and set the KS energy at zero. Σ^- is proportional to $n+1$, so the plateau is visible at low and high temperatures. Although the self-energy becomes larger with temperature, the spectral function is normalized, and there is little effect in the shape of the plateau. The spectral weight is essentially zero between $-\omega_{\mathrm{LO}}$ and the peak, indicating that the plateau is indeed given by the contribution of modes with $\omega\sim\omega_{\mathrm{LO}}$. As temperature increases, the distance from the QP peak to the plateau is very different from ω_{LO}. For Σ^+, which is proportional to n instead of $n+1$, there is no plateau at low temperatures. At $T = 900$ K, since $+\omega_{\mathrm{LO}}$ is about 1800 K (in temperature units), the plateau should be visible, but it coincides with the main peak, making the peak artificially wide at 900 K. At higher temperatures, the QP peak is shifted to larger values and the plateau acquires more weight, becoming visible. However, both the overlap of the plateau and main peak, and the varying distance between them, are artificial effects of the DM approach. In CE instead, plateaus (if visible) are at about $-\omega_{\mathrm{LO}}$ and $+\omega_{\mathrm{LO}}$ from the main peak.

For the CBM, Fig. S.6.2, the behavior is analogous, but the plateau and main peak never merge. The DM spectral function in Figs. 10 and 11 uses the full self-energy $\Sigma = \Sigma^- + \Sigma^+$.

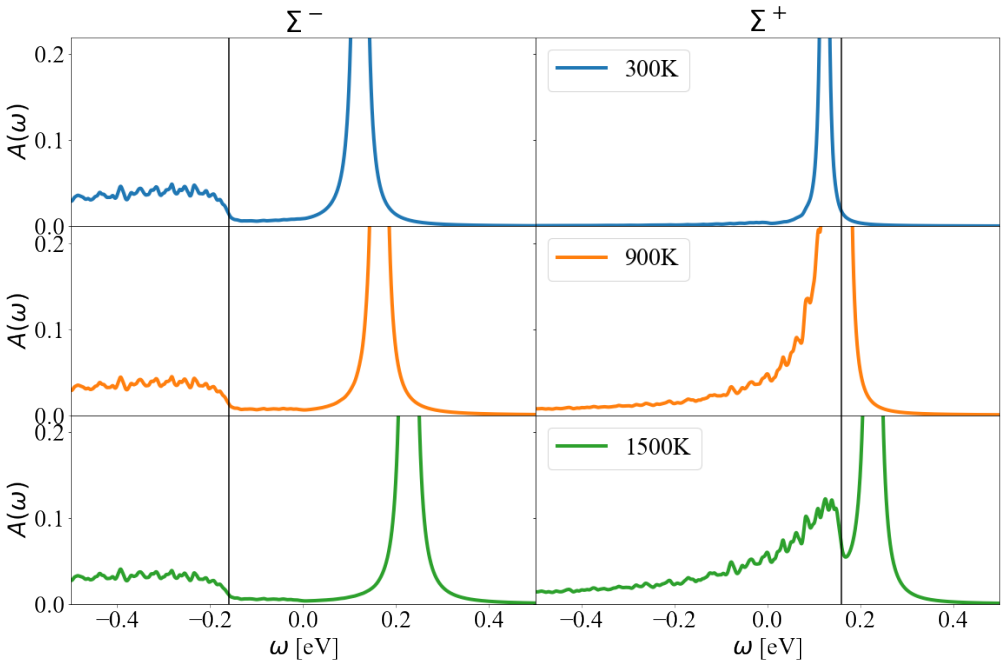

Figure S.6.1 The DM spectral function at the VBM splitted into Σ^{+} and Σ^{-} for T=300, 900, 1500 K, calculated with a $128 \times 128 \times 128$ $\mathbf{q}$-mesh and $\eta = 5$ meV. The vertical black lines in the figures show $-\omega_{LO}$ on the left and $+\omega_{LO}$ on the right.

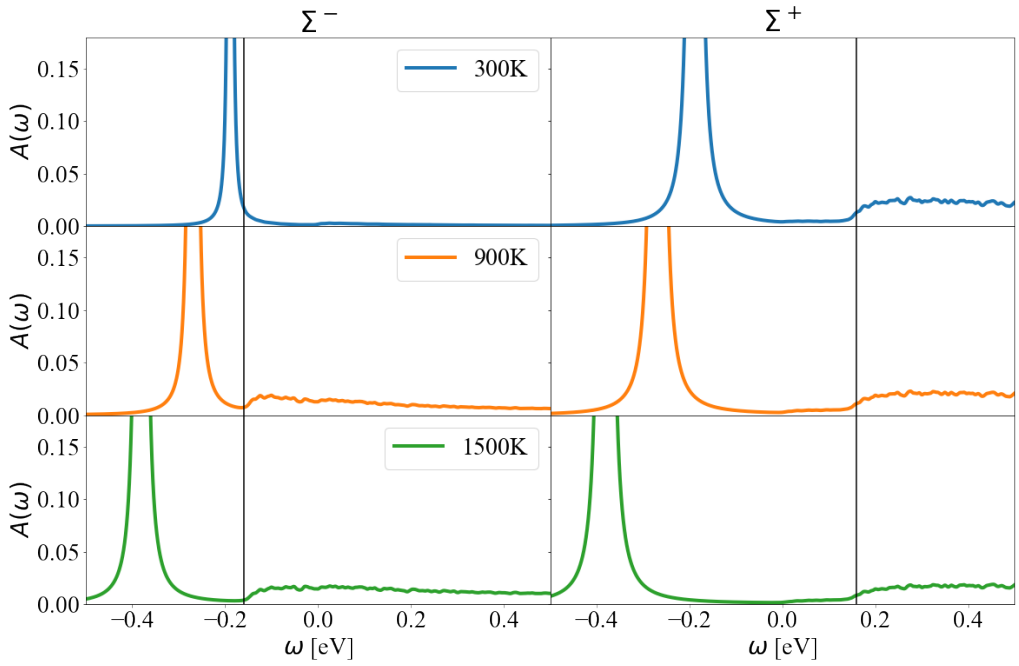

Figure S.6.2 The DM spectral function at CBM splitted into Σ^+ and Σ^- for T=300, 900, 1500 K, calculated with a $128 \times 128 \times 128$ $\mathbf{q}$-mesh and $\eta = 5$ meV. The vertical black lines in the figures show $-\omega_{LO}$ on the left and $+\omega_{LO}$ on the right.

S.6.3 Scattering matrix elements

The e-ph scattering matrix elements are obtained from the derivative of the KS potential. Although quadrupoles contribute to the KS potential around Γ, their contribution to the electron-phonon matrix elements is negligible, as can be observed in Fig. S.6.3. $|g_{CBM}(\mathbf{q})|$ is the sum of the matrix elements over all bands and phonon modes calculated at the CBM.

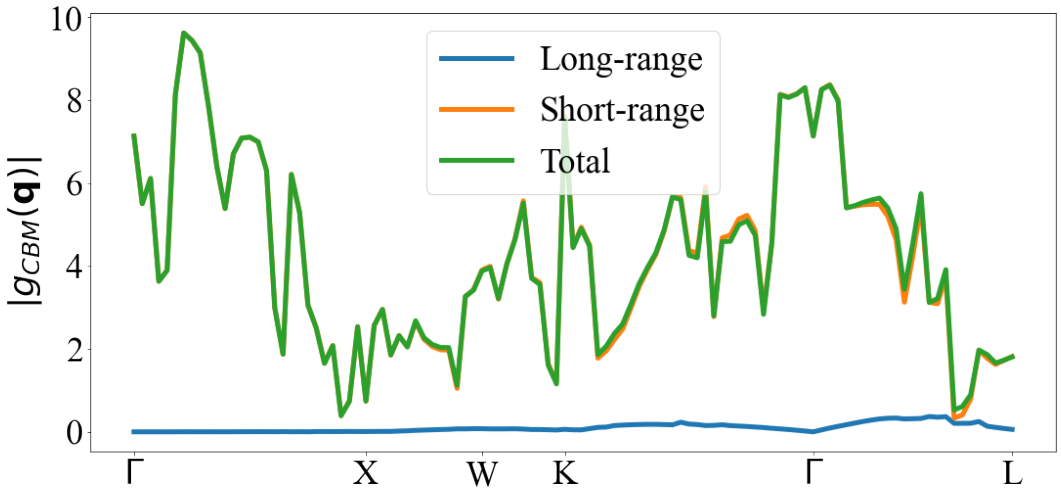

Figure S.6.3 Modulus of electron-phonon scattering matrix elements, $g^{j\mathbf{q}}_{nm\mathbf{k}}$, evaluated at $n\mathbf{k} =$ CBM and summed over the m bands and j phonon modes. These elements are pictured in a $\mathbf{q}$-path following high-symmetric crystal points in the reciprocal lattice. There is a split between long-range (blue) and short-range fields (orange), together with their sum (green). The long-range contribution to the electron-phonon scattering matrix elements, and, thus, to the nonpolaron plateau is negligible.

S.6.4 ARPES

Taking into account just the ARPES theoretical picture, Fig. S.6.4, it is difficult to discern changes between DM and CE approaches at 300 K, Fig. S.6.4a. As the temperature is increased to 900 K, Fig. S.6.4b, or 1500 K, Fig. S.6.4c, one can notice a shift and broadening of the bands, in particular at the CBM between Γ and X points and the VBM at Γ point. The horizontal lines visible at 8 eV and (less visible) at -3 eV, corresponding to a very small peak in the spectral function, are due to the high density of states at the band extrema at L.

Notes and references

[1] W. Kohn and L. J. Sham, *Physical Review*, 1965, **140**, A1133.

[2] R. M. Martin, *Electronic Structure: Basic Theory and Practical Methods*, Cambridge University Press, 2004.

[3] X. Gonze and C. Lee, *Physical Review B*, 1997, **55**, 10355.

[4] J. P. Perdew and A. Zunger, *Physical Review B*, 1981, **23**, 5048.

[5] J. P. Perdew and Y. Wang, *Physical Review B*, 1992, **45**, 13244.

[6] M. van Setten, M. Giantomassi, E. Bousquet, M. Verstraete, D. Hamann, X. Gonze and G.-M. Rignanese, *Computer Physics Communications*, 2018, **226**, 39.

[7] A. H. Romero and *et al*, *The Journal of Chemical Physics*, 2020, **152**, 124102.

[8] X. Gonze and *et al*, *Computer Physics Communications*, 2020, **248**, 107042.

[9] S. Stoupin and Y. V. Shvyd'ko, *Physical Review Letter*, 2010, **104**, 085901.

[10] S. Logothetidis, J. Petalas, H. M. Polatoglou and D. Fuchs, *Physical Review B*, 1992, **46**, 4483.

[11] S. Poncé, F. Macheda, E. R. Margine, N. Marzari, N. Bonini and F. Giustino, *Physical Review Research*, 2021, **3**, 043022.

[12] X. Gonze, P. Boulanger and M. Côté, *Annalen der Physik*, 2010, **523**, 168–178.

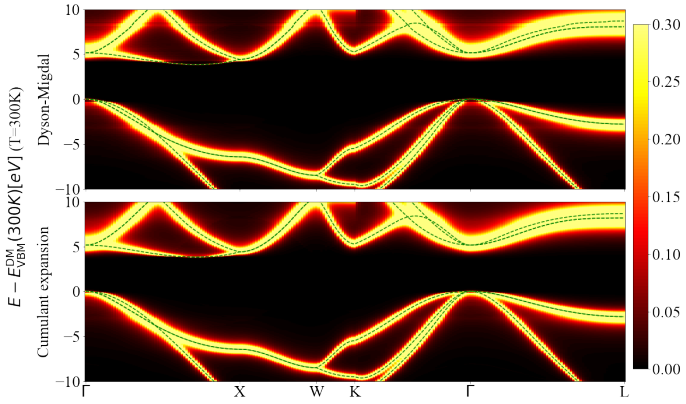

(a) $T = 300K$

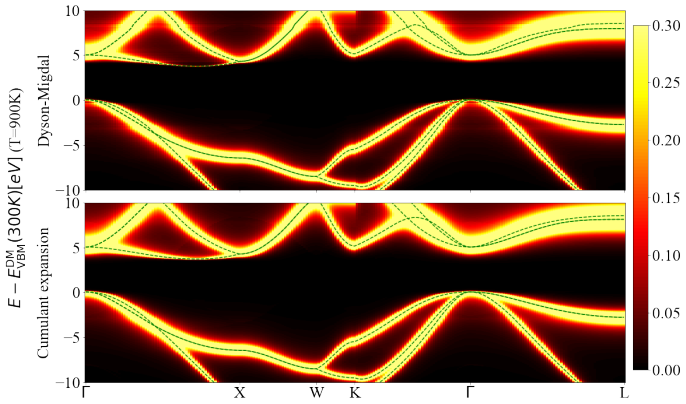

(b) $T = 900K$

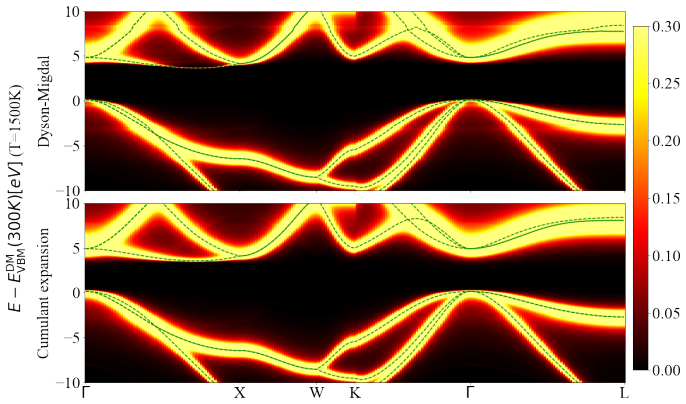

(c) $T = 1500K$

Figure S.6.4 Spectral function at 300 K (top), 900 K (middle), and 1500 K (bottom). The calculations were performed using DM (top in each figure) and CE (bottom in each figure) with a $N = 128$ $\mathbf{q}$-grid. All values were displaced in relation to the VBM at 300 K. To be able to observe the presence of the nonpolaron signature near VBM and CBM, the intensity scale of the density of states (colormap) was limited to 0.3.